Evaluation of Liquefaction Potential of Impounded Fly Ash

Behrad Zand[1*], Wei Tu[2], Pedro J. Amaya[3], William E. Wolfe[4], Tarunjit Butalia[5]

[1]Graduate Research Associate, Department of Civil and Environmental Engineering and Geodetic Science, The Ohio State University, 470 Hitchcock Hall, 2070 Neil Ave., Columbus, OH 43210, US, Tel: (614) 292-0992, Fax: (614) 292-3780, E-mail: zand.3@osu.edu

[2] PE, Graduate Research Associate, Department of Civil and Environmental Engineering and Geodetic Science, The Ohio State University, E-mail: tu.45@osu.edu

[3] PE, Senior Geotechnical Engineer, Civil Engineering Division, American Electric Power, Service Corporation, 1 Riverside Plaza, Columbus, OH 43215-2373, US, Tel: (614) 716-2926, E-mail: pjamaya@aep.com

[4] PhD, PE, Professor, Department of Civil and Environmental Engineering and Geodetic Science, The Ohio State University, Tel: (614) 292-0790, E-mail: wolfe.10@osu.edu

[5] PhD, PE, Research Scientist, Department of Civil and Environmental Engineering and Geodetic Science, The Ohio State University, E-mail: butalia.1@osu.edu

[*] Corresponding author

Abstract

An experimental and analytical investigation of the liquefaction potential of Class F fly ash is presented. The fly ash, originally placed in a 45 hectares impoundment, varied in depth from about 15 to 55 m. The proposed use for the ash was as a base for a utility monofill. The evaluation included cyclic triaxial tests performed on reconstituted fly ash samples at different densities, confining stresses and cyclic stress ratios representative of the impounded material and the seismic environment. Post-liquefaction strengths were measured by reconsolidating the samples at the initial effective confining stress and performing consolidated undrained (CU) triaxial tests. The measured cyclic strength was compared with the seismically induced stresses in the profile using the well known one dimensional wave propagation program SHAKE. The cyclic loadings imposed on the ash by the design earthquakes were found to be lower than the measured cyclic strength of the fly ash material.

Key Words: Impounded Fly Ash, Liquefaction Potential, Dynamic Triaxial Test, Harvard Miniature Mold

1. Introduction

Utilization and/or disposal of high volume coal combustion products combined with the increasing environmental restrictions and rising land filling costs have became major concerns for utilities. American Coal Ash Association survey[1] estimates the total fly ash production in US to be 65 million tons (71 million US tons) in 2005, from which only 41% was reused and the rest was left to be disposed in storage ponds or landfills. To exploit its full capacity, a 45 hectares fly ash impoundment owned by American Electric Power (AEP) was proposed as the base for a utility monofill. The liquefaction potential of fly ash

during earthquake was a concern of the design team. Although a large amount of literature exists on the cyclic resistance of sands and clayey soils (Ref. 2 to 9) little has been done to determine the liquefaction potential of fly ash. To address this concern an experimental program along with an analytical study was conducted to evaluate the liquefaction potential of the material and the post liquefaction shear strength. The cyclic strength of the fly ash material was measured using standard cyclic triaxial test according to ASTM D5311[10], and the initial and post liquefaction shear strengths were evaluated using undrained shear (CU) test[11].

2. Testing Procedures and Specimen Preparation

Fly ash samples were made using wet tamping method. Target dry densities were 86%, 95%, and 105% of the optimum standard Procter dry density[12]. Specimens were consolidated under effective stresses of 68, 135, and 340 kPa, representing typical depths of about 3.5, 7, and 20 m, respectively. The specimens were tested under cyclic shear stress ratios ranging from 7.5 to 40% of the effective confining stress. Consolidated undrained (CU) tests were performed to establish the initial static undrained shear strength of the fly ash material. Additional post-liquefaction CU test was conducted to determine the static undrained shear strength after the earthquake event.

a) Material Properties

Class F fly ash produced by AEP's Mitchell power plant in Ohio was used in this study. Fly ash samples were collected from a 45 hectare impoundment varying in depth from about 15 to 55 m. A gradation curve, supplied by AEP, is presented in Figure 1. A specific gravity of 2.27 was measured by AEP. The in-situ density of the material was determined by AEP to range from 1600 to 1680 kg/m^3 with a moisture content of about 30%. The

in-situ dry density of the material is estimated to range from 92% to 96% of the optimum Proctor dry density.

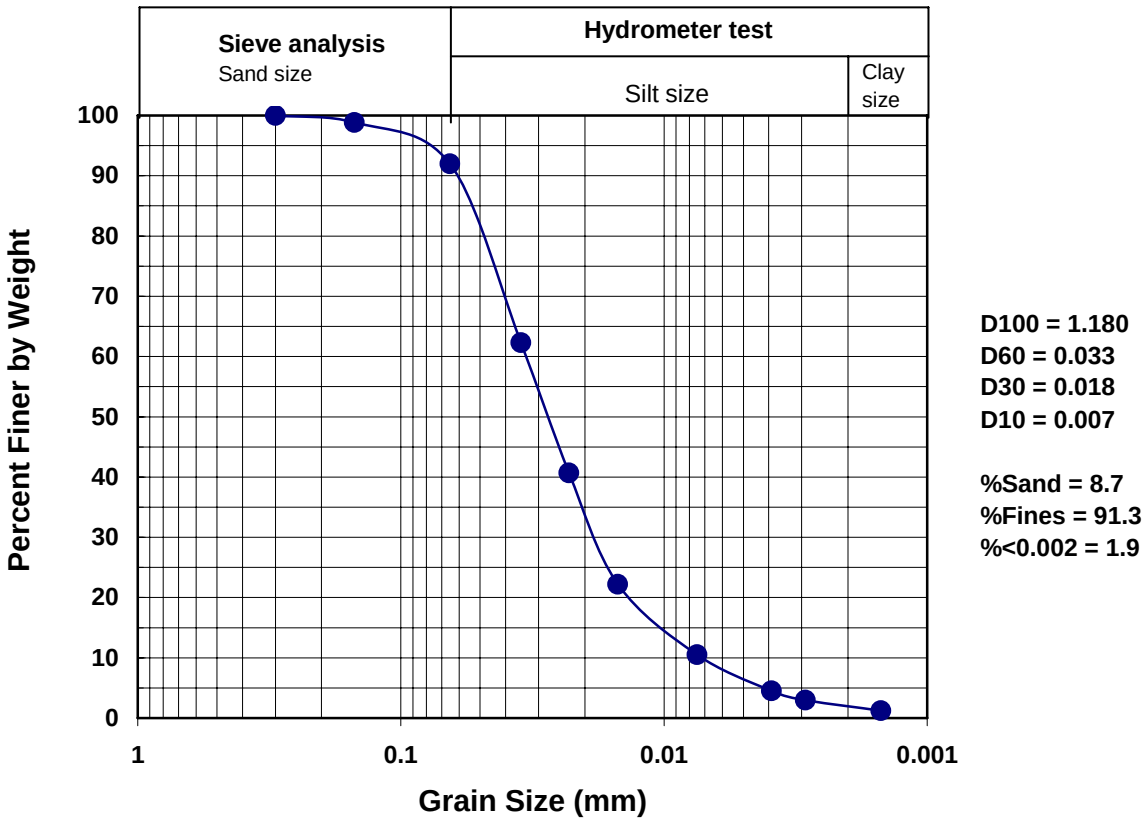

Figure 1. Grain size distribution of fly ash

b) Specimen Preparation

Harvard Miniature samples (3.35 cm diameter, 7.11 cm length) were compacted in five equal lifts using a 110 N (25 lb) hand tamper. Figure 2 shows a comparison between the

standard Proctor curve and the Harvard miniature calibration curve. Saturation of the specimens were achieved by application of a small vacuum pressure (<60 kPa) followed by a back pressure of 105 to 310 kPa. To improve saturation, a low pressure gradient was applied from bottom to the top. Saturation was determined by measuring the B-value and all the specimens tested possessed a B-value larger than 97%. The average time needed to saturate the specimens varied from one 24 hrs to two weeks.

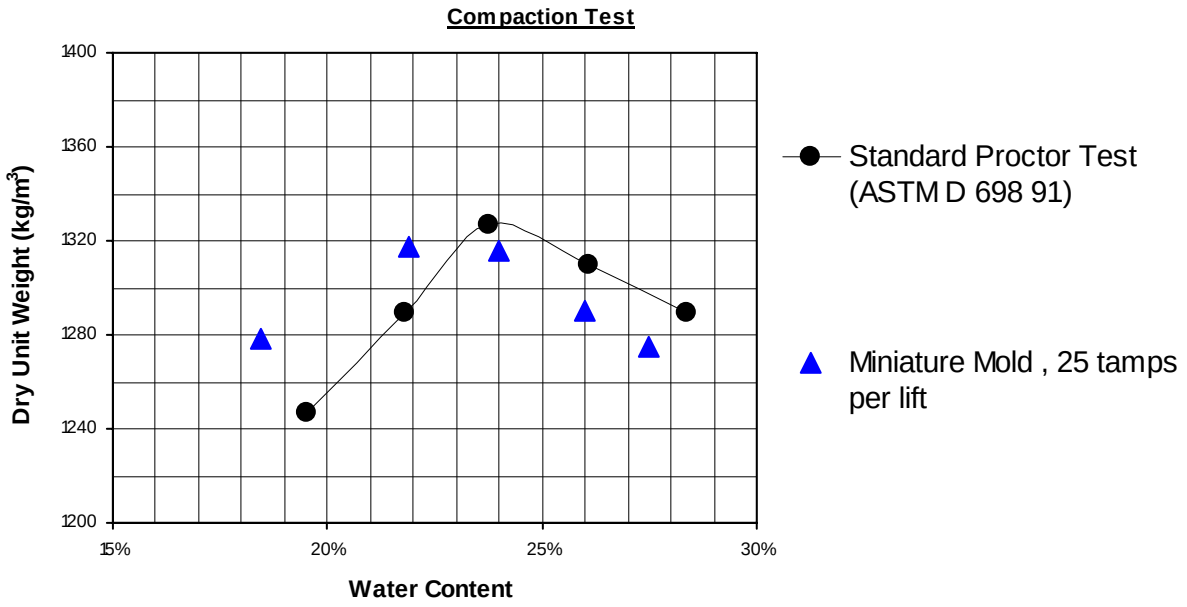

Figure 2. Calibration of compaction effort for Harvard Miniature samples

c) Cyclic Triaxial Test

Cyclic tests were performed using an MTS load frame. A 450 Newton load cell was used to control load cycles in load control mode while axial deformations were measured by a

LVDT attached to loading piston. Each saturated specimen was consolidated under the desired effective confining pressure. Due to the high permeability of the samples (of the order of 10^{-4} cm/sec) the consolidation typically occurred quickly. The cyclic test was conducted under undrained conditions and constant cell pressure. Sample pore water pressure and deformation, as well as the deviator load were recorded continuously at a sampling rate of 100 Hz. Various effective stresses and shear stress ratios were tested to develop cyclic strength curves. The loading frequency was selected to be 0.5 Hz except for one case where a frequency of 1 Hz was used. During a cyclic test, the specimen pore water pressure increased with a rate that was a function of cyclic stress ratio, relative density, and effective confining pressure. Liquefaction was defined as the point at which the excess pore water pressure reached the asymptotic level of the initial effective confining pressure accompanied with a dramatic increase in the axial deformation (Figure 3).

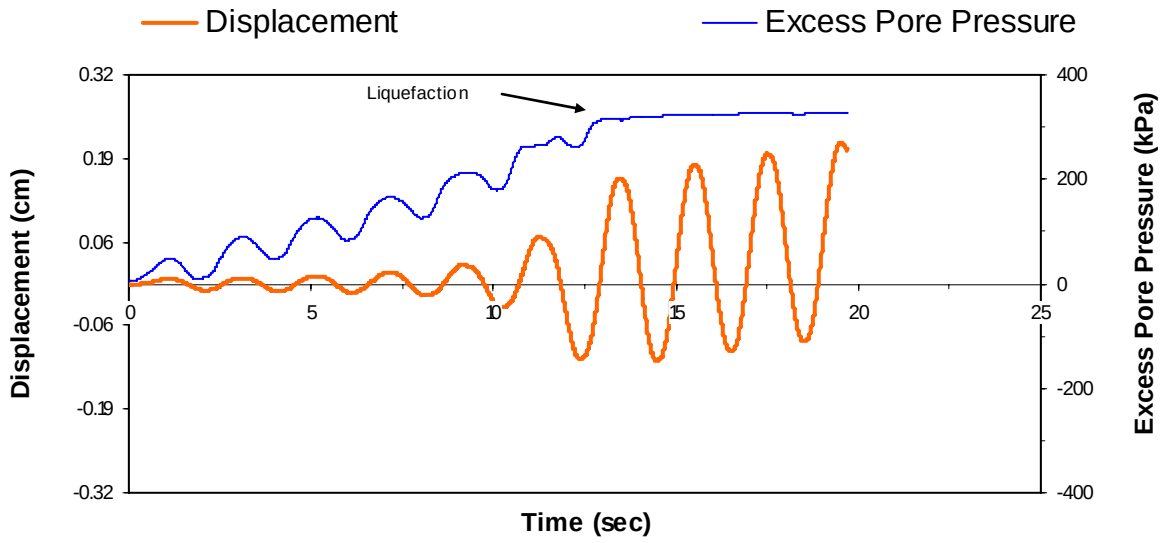

Figure 3. Identification of liquefaction for cyclic triaxial tests

d) *Consolidated Undrained Shear Test*

The undrained shear strength was measured after liquefaction in accordance with ASTM D4767[11] with pore water pressure measurement using a strain control Instron load frame.

3. Results and Discussion

a) Laboratory testing

Presented in Table 1 is a list of the specimens tested under cyclic loading together with their relative dry density, effective confining pressure, and shear stress ratios (deviator stress divided by twice effective stress). Figure 4 shows the cyclic test results for the fly ash specimens compacted to 95% of the standard Proctor density. The number of loading cycles to produce liquefaction is seen to decrease with increasing shear stress ratio and increasing confining stress. The two curves that represent 135 and 340 kPa effective confining stresses are very close, suggesting that as confining stress increases liquefaction resistance becomes less sensitive to the confining stress.

In Figure 5 the results of the liquefaction tests conducted on specimens subjected to an initial confining stresses of 135 kPa are presented. Here it is apparent that the liquefaction resistance increases with increasing initial density.

Sample ID	Initial Compaction	Nominal Confining Stress (kPa)	$\frac{\sigma_d}{2\sigma_C}$
85C-135-8 *	87%	135	7.5%
85C-135-10*	86%	135	10%
85C-135-13 *	86%	135	13%
85C-135-15	85%	135	15%
85C-135-20*	86%	135	20%
95C-68-16 *	95%	68	16%
95C-68-17	96%	68	17%
95C-68-18	96%	68	18%
95C-68-20 *	95%	68	20%
95C-68-21	95%	68	21%
95C-68-40	94%	68	40%
95C-135-10	95%	135	10%
95C-135-11	96%	135	11%
95C-135-13 *	95%	135	13%
95C-135-15	95%	135	15%
95C-135-21 *	95%	135	21%
95C-135-25	95%	135	25%
95C-340-10 *	95%	340	10%
95C-340-11	95%	340	11%
95C-340-15	95%	340	15%
95C-340-20	95%	340	20%
95C-340-37	95%	340	37%
105C-135-20 *	104%	135	20%

* Post-liquefaction CU test conducted

Table 1. List of specimens and loading conditions for cyclic tests

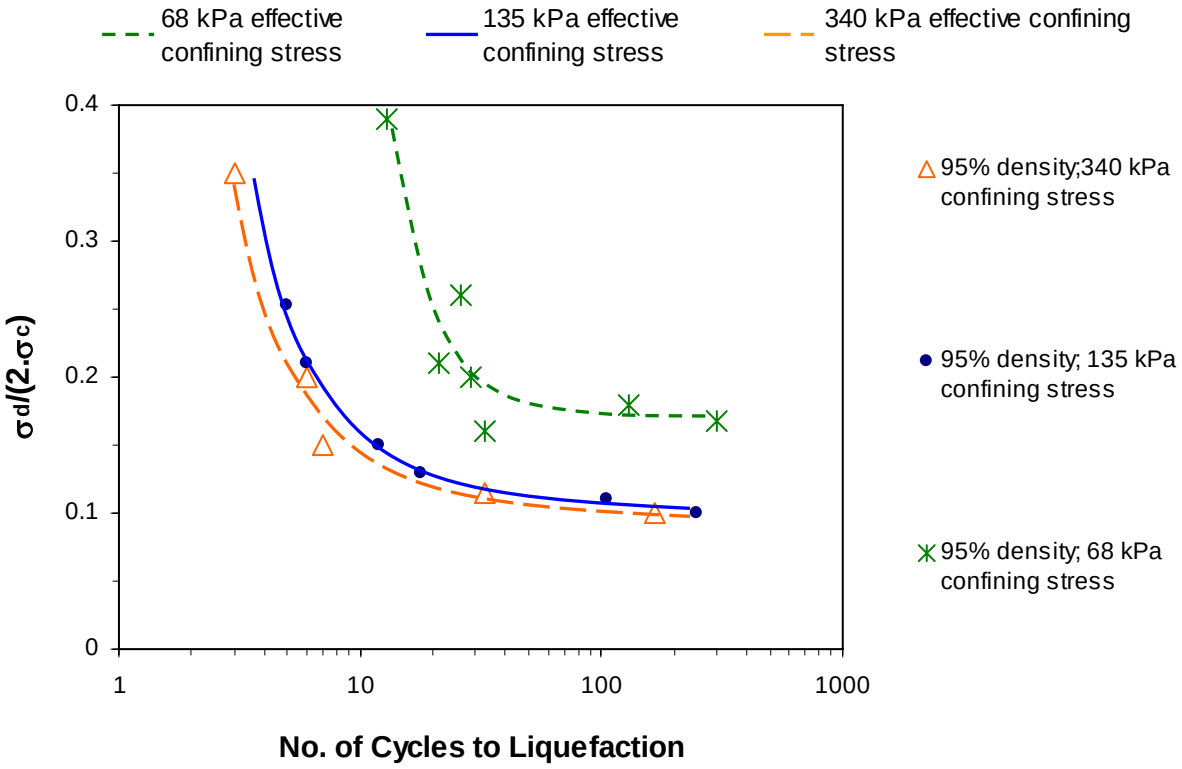

Figure 4. Laboratory cyclic test results for 95% compacted specimens showing effect of confining stress on liquefaction resistance

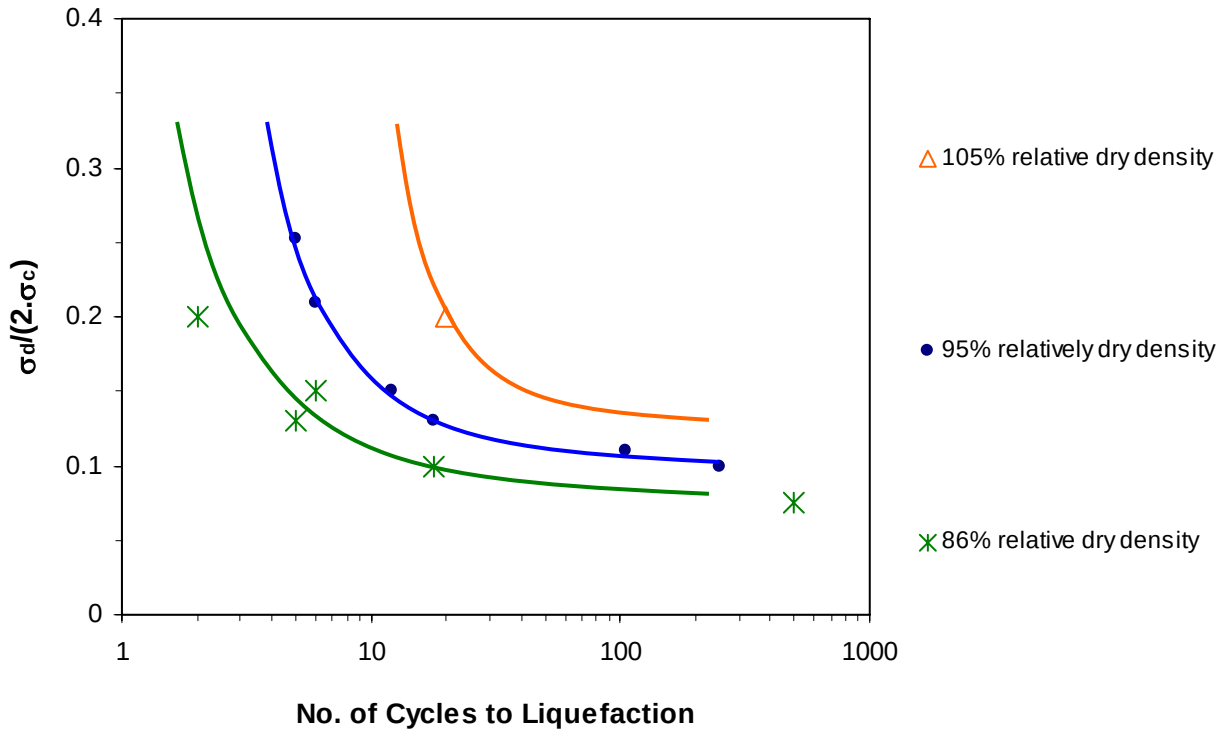

Figure 5. Laboratory cyclic test results for confining stress of 135 kPa showing effect of density on liquefaction resistance

After liquefaction, selected specimens were re-consolidated to the initial effective confining stress and the post-liquefaction undrained shear strengths were measured. Table 2 presents a summary of these test results. This table also includes the number of cycles applied together with the maximum axial strain experienced during the cyclic test. Figure 6 presents examples of two typical deviator stress versus axial strain curves for these samples. In the first example, an initial peak in shear strength at a relatively low axial strain (less than 2%) is apparent. The peak is followed by an increase in the shear strength at higher axial strains. The second example has a peak at a relatively high shear strain, associated with a negative excess pore water pressure.

Table 3 presents summary results of undrained shear test results conducted to measure initial shear strength of the fly ash material. The initial dry densities for the first two specimens were 86% and 95% relative to the standard optimum Proctor density. That for the last two specimens was 105%. The 86% relative density specimen was tested under 103 kPa of effective confining stress and the rest of the specimens under about 137 kPa. Comparison between initial and post-liquefaction undrained shear strengths for specimens with low compaction degree indicates a slight decrease in the peak shear strength, along with significant increases in the residual shear strength after liquefaction. The characteristic of the shear stress versus axial strain curve changes after liquefaction, as the initial shear strength of the specimens exhibits a peak; then it quickly drops to a residual value. The post-liquefaction shear strength, however, shows an increasing trend for high axial strains. For highly compacted specimens the post liquefaction shear strength decreases slightly but the general trend of the stress-strain curves remains similar.

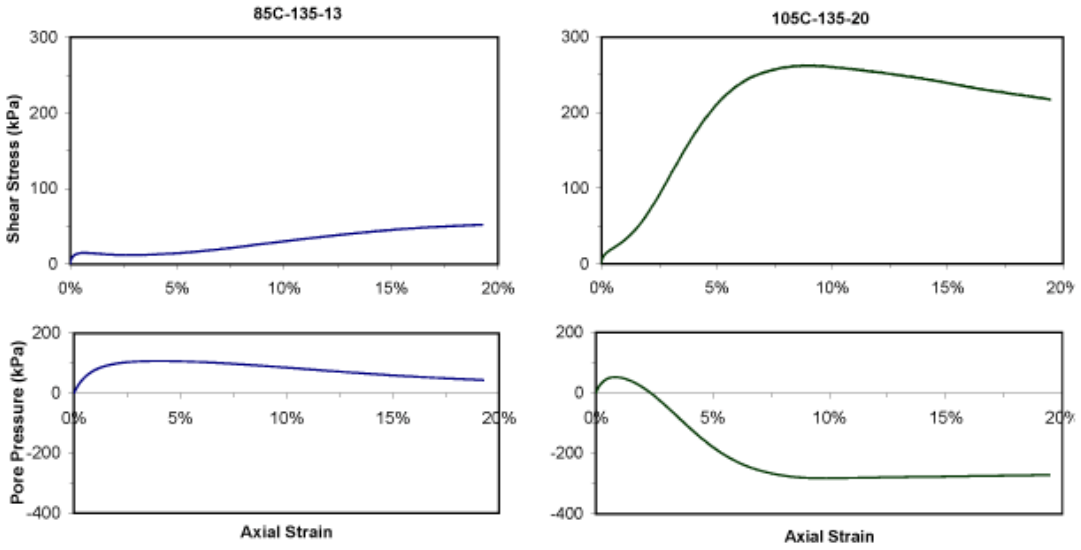

Figure 6. Typical stress-strain curves for post-liquefaction undrained shear tests

Sample ID	No. of Cycles Applied	Max Axial Strain Experienced	Undrained Shear Strength						
			Peak Shear Strength			5% Axial Strain		10% Axial Strain	
			τ (kPa)	Axial Strain	u^* (kPa)	τ (kPa)	u (kPa)	τ (kPa)	u (kPa)
85C-135-10	23	1.1%		No peak		44.8	42.1	62.7	16.5
85C-135-8	500	0.7%	17.9	0.49%	50.3	4.4	117.9	4.4	118.6
85C-135-13	9	3.6%	15.2	0.54%	54.6	14.5	106.2	30.3	85.5
85C-135-20	5	2.2%	22.1	1.15%	75.8	22.1	95.1	24.1	-2.6
95C-68-15	39	6.3%		No peak		20.7	36.5	49.0	-5.5
95C-68-20	32	1.3%		No peak		66.9	12.4	68.2	12.4
95C-135-20	12	3.9%	10.3	0.64%	71.0	113.8	4.8	106.9	7.6
95C-135-13	24	2.9%	19.3	2.00%	82.9	14.5	98.6	20.0	92.4
95C-340-10	171	2.5%		No peak		306.1	-35.2	362.7	-112.4
105C-135-20	28	1.4%		No peak		211.0	-177.9	260.0	-282.0

* u represents specimen pore water pressure

Table 2. Post liquefaction undrained shear strength

Sample ID	Effective Confining Stress (kPa)	Undrained Shear Strength						
		Peak Shear Strength			5% Axial Strain		10% Axial Strain	
		τ (kPa)	Axial Strain	u (kPa)	τ (kPa)	u (kPa)	τ (kPa)	u (kPa)
85C-100-CU	103	22.8	0.65%	50.9	10.8	95.3	9.9	97.6
95C-135-CU	135	24.2	0.79%	66.2	7.0	113.8	3.72	120.6
105C-135-CU	135	250.3	4.15%	-140.0	250.3	-149.6	222.0	-140.0
105C-131-CU	131	257.9	5.17%	-150.5	256.5	-147.5	237.9	-154.4

Table 3. Initial undrained shear strength test results. The presented shear strengths are effective values

b) Ground Response Analysis

A ground response analysis was performed using the program SHAKE[13] which is a one-dimensional equivalent linear wave propagation analysis. The analysis was carried out for two critical sections. Based on the results of laboratory and subsurface investigation programs two critical profiles were developed for the Mitchell Station. Site characterization included thickness and unit weight for each soil layer present at the site, and estimates of the dynamic soil properties (shear modulus or shear velocity, modulus reduction and damping models). Appropriate earthquake (natural or synthetic) input motions were selected to represent the design bedrock motion for the site.

The two soil profiles, A-A' and B-B', and their dynamic properties are presented in Tables 4 and 5, respectively. The maximum shear modulus of each layer was estimated based on empirical relationships presented in the literature. The maximum shear modulus of sand was assumed to be a function of density and confining stress[14]. For the fine grain materials, the maximum shear modulus was estimated from the undrained shear strength and the subsurface investigation results[14,15], where published shear wave velocities were used to estimate the maximum shear modulus of the sandstone bedrock[16]. In most engineering applications, standard curves for various basic soil types are used in the analysis although site specific curves can be derived from laboratory tests[15]. In this study, standard curves were chosen based on the soil type (Tables 4 and 5). Since no specific curves for fly ash materials are available, the curves developed for sands were selected rather than clay to reflect that the fly ash is non-plastic. The unit weight of each layer was determined based on the given subsurface investigation results. The depths of ground water table for the two soil profiles were investigated by AEP as observed in the ground water monitoring well data. Two natural earthquake input motions, El Centro and Taft, were selected to represent the design bedrock motion at the

site. The peak accelerations of the input motions were scaled to match the design accelerations of 0.08g and 0.15g as specified by AEP.

Eight analyses were performed using the two selected input motions and the two design peak accelerations (Table 6). Output from the program included the time histories of acceleration, velocity, displacement, shear strain, and shear stress on the top three fly ash layers and ground surface. The common cyclic stress approach was used for liquefaction potential evaluation. In this approach, the earthquake-induced loading is compared with liquefaction resistance of the soil expressed in terms of cyclic shear stresses [15]. In order to compare with the cyclic strength determined in laboratory tests, the transient and irregular time history of earthquake-induced shear stresses obtained from the ground response analyses were converted into an equivalent series of uniform stress cycles. The equivalent number of uniform stress cycles (N_{equ}) was determined by counting the stress cycles with amplitude greater than 65% of the peak cyclic shear stress ($\tau_{\max}$) for a particular shear stress time history as [17]:

$$\tau_{cyc} = 0.65\tau_{\max} \qquad \text{Equation 1}$$

Although different stress levels have been developed for this approach[18], 65% is most commonly used[15]. The uniform shear stress is typically normalized by the initial overburden stress to produce a cyclic stress ratio (CSR):

$$CSR = \frac{\tau_{cyc}}{\sigma_0'} \qquad \text{Equation 2}$$

Earthquakes generally produce shear stresses in different directions. Pyke et al.[19]

showed that multidirectional shaking can cause pore water pressure to increase more rapidly than single unidirectional shaking. Previous work by other researchers has shown[20] that the CSR required to produce initial liquefaction in the field is about 10% less than values measured in the laboratory. Therefore, the predicted field cyclic stress ratio from ground response analysis was corrected based on the relationship as follows:

$$(CSR)_{field} = 0.9(CSR)_{lab} \qquad \text{Equation 3}$$

The ground response analyses results are summarized in Table 7. The predicted maximum cyclic stress ratio of 0.14 was obtained from the analysis on the B-B' profile with Taft earthquake input motion at a peak acceleration of 0.15g. Figure 7 presents a comparison between the design earthquake loading predicted from the numerical analysis and the experimentally obtained cyclic strengths. The solid lines represent the laboratory obtained data for 135 kPa effective confining pressure for the three different relative densities of 86%, 95%, and 105%.

The in-situ density of the material was estimated to range from 92% to 96% relative to the optimum Proctor density. Comparison between the numerical results and experimental liquefaction potential curve for 95% relative density and 135 kPa confining stress shows that the material has sufficient strength during the design earthquakes and will not liquefy.

Layer No.	Material Description	H (m)	γ (kg/m^3)	G_x (MPa)	Vs (m/sec)	Modulus Reduction & Damping Curve
1	Recompacted Clay Liner	3	2000	26786	304.8	Clay[21]
2	Drainage layer	2.4	2000	22750	280.7	Sand – Average[22]
3	Fly ash	3	1600	6895	172.8	Sand – Average[22]
4	Fly ash	3	1600	8273	189.2	Sand – Average[22]
5	Fly ash	5.5	1600	9653	204.5	Sand – Average[22]
6	Fly ash	9.1	1600	11032	218.5	Sand – Average[22]
7	Fly ash	9.1	1600	12410	232.0	Sand – Average[22]
8	Fly ash	9.1	1600	13100	238.0	Sand – Average[22]
9	Fly ash	9.1	1600	13790	244.4	Sand – Average[22]
10	Sandstone	∞	2245	9.3E6	1700	Linear

Table 4. Site characteristics of soil profile A-A'

Layer No.	Material Description	H (m)	γ (kg/m^3)	G_x (MPa)	Vs (m/sec)	Modulus Reduction & Damping Curves
1	Recompacted Clay Liner	5.5	2000	26786	304.8	Clay[21]
2	Drainage layer	2.8	2000	27579	309.1	Sand – Average[22]
3	Fly ash	3.0	1600	6895	172.8	Sand – Average[22]
4	Fly ash	3.0	1600	8273	189.3	Sand – Average[22]
5	Fly ash	6.1	1600	9653	204.5	Sand – Average[22]
6	Fly ash	6.1	1600	11032	218.5	Sand – Average[22]
7	Fly ash	9.8	1600	12410	232.0	Sand – Average[22]
8	Sandstone	∞	2245	9.3E6	1700	Linear

Table 5. Site characteristics of soil profile B-B'

Analysis No.	Site Profile	Input Earthquake	Peak Acceleration %g
A1	A-A’	Taft	8
A2	A-A’	Taft	15
A3	A-A’	El Centro	8
A4	A-A’	El Centro	15
B1	B-B’	Taft	8
B2	B-B’	Taft	15
B3	B-B’	El Centro	8
B4	B-B’	El Centro	15

Table 6. Input earthquake motions

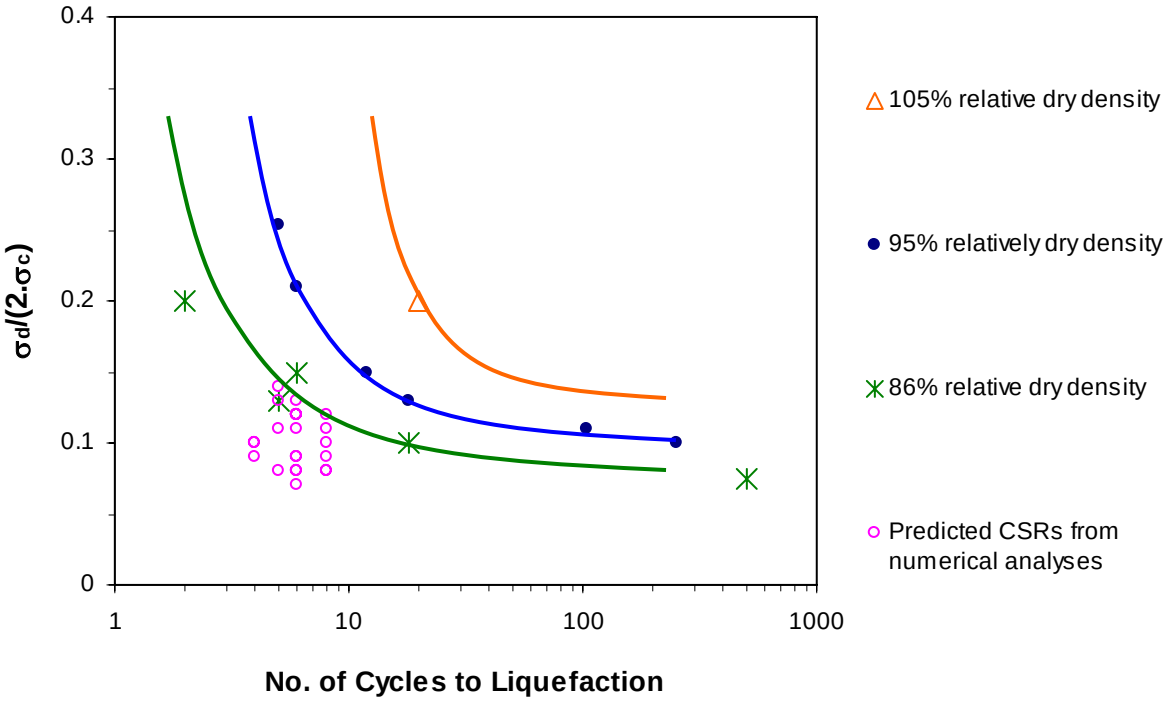

Figure 7. Comparison between the design earthquake load and cyclic resistance of fly ash

Parameters	Layer #	Depth (m)	σ_0' (kPa)	τ_{max} (kPa)	τ_{cyc} (kPa)	N_{equ}	CSR
A-A'	3	5.5	107.7	14.84	2.67	4	0.09
Taft	4	8.6	155.6	20.88	13.55	4	0.09
a_{max}=0.08g	5	11.6	203.5	25.66	16.66	4	0.08
A-A'	3	5.5	107.7	19.00	12.35	6	0.11
Taft	4	8.5	155.6	26.62	12.28	6	0.11
a_{max}=0.15g	5	11.6	203.5	32.65	21.21	6	0.10
A-A'	3	5.5	107.7	13.36	8.67	8	0.08
El Centro	4	8.5	155.6	18.29	11.87	8	0.08
a_{max}=0.08g	5	11.6	203.5	21.92	14.27	8	0.07
A-A'	3	5.5	107.7	18.48	12.02	6	0.11
El Centro	4	8.5	155.6	25.66	16.66	6	0.11
a_{max}=0.15g	5	11.6	203.5	31.36	20.40	6	0.10
B-B'	3	7.9	155.6	19.49	12.69	6	0.08
Taft	4	11.0	203.5	23.94	15.56	6	0.08
a_{max}=0.08g	5	14.0	251.4	25.90	16.85	6	0.06
B-B'	3	7.9	155.6	29.68	19.30	5	0.12
Taft	4	11.0	203.5	36.15	23.51	5	0.12
a_{max}=0.15g	5	14.0	251.4	38.59	25.09	5	0.10
B-B'	3	7.9	155.6	18.82	12.21	6	0.08
El Centro	4	11.0	203.5	23.65	15.40	5	0.08
a_{max}=0.08g	5	14.0	251.4	26.43	17.19	6	0.07
B-B'	3	7.9	155.6	26.43	17.19	8	0.11
El Centro	4	11.0	203.5	30.98	20.16	8	0.10
a_{max}=0.15g	5	14.3	251.4	34.33	22.31	8	0.09

Table 7. Summary of the ground response analyses results

4. Summary and Conclusions

In this study, the liquefaction potential of an impounded fly ash material was investigated. Cyclic triaxial tests were performed on reconstituted samples with different relative densities, confining stresses, and shear stress ratios. The cyclic shear strength of the fly ash material was presented graphically in terms of cyclic strength curves which show the relationship between density, cyclic stress amplitude, and number of cycles to liquefaction. After cyclic triaxial tests, some of the specimens were reconsolidated to the initial effective confining stress and subjected to consolidated undrained (CU) triaxial tests. Additional CU tests were performed to determine the initial static undrained shear strength. The design seismic loading in terms of cyclic stress ratio and equivalent number of cycles were obtained from ground response analyses. The liquefaction potential of the fly ash material was evaluated based on the comparison of the cyclic strength and design earthquake loading. It was concluded that:

1. The cyclic loading imposed by the design earthquakes was found to be lower than the cyclic strength of the fly ash material.
2. Liquefaction resistance of the material (maximum shear stress ratio for a given number of cycles) was found to be a strong function of initial dry density.
3. In addition to dry density, the liquefaction resistance was found to be influenced by the effective stress at low levels of effective stress. Cyclic behavior of field material was represented by the specimens consolidated under higher effective stresses.

5. Acknowledgement

AEP suggested the topic of this study and provided the material and classification test data. The authors would like to thank AEP for its support during this investigation. The

authors would also like to acknowledge Singh Gursimran Singh for his contribution to the lab work.

6. List of References

1. ACAA 2005 Coal Combustion Products Survey Findings, American Coal Ash Association, 2005.
2. Seed, H.B., and Idriss, I, M., “Ground motions and soil liquefaction during earthquakes,” Monograph series, Earthquake Engineering Research Institute, Berkly, Calif, 1982.
3. Seed, H. B., Tokimatsu, K., Harder, L. F., and Chung, R. M., “Influence of SPT procedures in soil liquefaction resistance evaluations,” Journal of Geotechnical Engineering, Vol. 111, No. 12, pp.1425-1445, 1985.
4. Sivathayalan, S., “Static, cyclic, and post liquefaction simple shear response of sands”, MSc thesis, The University of British Columbia, B.C., Canada, 1985.
5. Boulanger, R. and Seed, R. B., “Liquefaction of sand under bidirectional monotonic and cyclic loading”, Journal of Geotechnical Engineering, Vol. 12, No. 2, pp. 870-878, 1995.
6. Youd, T. L. and Idriss, I. N., NCEER. Proceedings Workshop on Evaluation of Liquefaction Resistance of Soils, Technical Report No. NCCER-97-0022, National Center for Earthquake Engineering Research, University of Buffalo, Buffalo, New York, 1997.
7. Finn W. D. L., “State-of-the-art of geotechnical earthquake engineering practice”, Soil Dynamics and Earthquake Engineering, Vol. 20, pp. 1-15, 2000.
8. Xenaki, V. C., and Athanasopoulos, G. A., “Liquefaction resistance of sand-silt mixture: an experimental investigation of the effect of fines”, Soil Dynamics and Earthquake Engineering, Vol. 23, No. 3, pp. 183-194, 2003.

9. Ghionna, V. N. and Porcino, D., “Liquefaction resistance of undisturbed and reconstituted samples of a natural coarse sand from undrained cyclic triaxial tests”, Journal of Geotechnical and Geoenvironmental Engineering, Vol. 132, No. 2, pp. 194-202,2006.
10. ASTM Designation: ASTM D5311, “Standard Test Method for Load Controlled Cyclic Triaxial Strength of Soil”, Annual Book of ASTM Standards, 2004, pp. 1167-1176.
11. ASTM Designation: ASTM D4767, “Standard Test Method for Consolidated Undrained Triaxial Compression Test for Cohesive Soils”, Annual Book of ASTM Standards, 2004, pp. 913-925.
12. ASTM Designation: ASTM D698, “Standard Test Method for Laboratory Compaction Characteristics of Soil Using Standard Effort”, Annual Book of ASTM Standards, 2002, pp. 78-85.
13. Schnabel, P. B., Lysmer, J. and Seed, H. B., “SHAKE – A computer program for earthquake response analysis of horizontally layered sites,” EERC Report 72-12. Earthquake Engineering Research Center, Berkeley, California, 1972.
14. Seed, H. B. and Idriss, I. M., “Soil Moduli and Damping Factors for Dynamic Response Analysis,” Report No. UCB/EERC-70/10, Earthquake Engineering Research Center, University of California, Berkeley, 1970.
15. Kramer, S.L. (1996). Geotechnical Earthquake Engineering, Prentice Hall, Inc., Upper Saddle River, New Jersey, 653 pp.
16. Burger, H. R., Exploration Geophysics of the Shallow Subsurface, Prentice Hall: Englewood Cliffs, NJ, 1992.
17. Seed, H.B., K. Mori and C.K. Chan, “Influence of Seismic History on the Liquefaction Characteristics of Sands”, Report No. UCB/EERC-75/25, Earthquake Engineering Research Center, University of California, Berkeley, 1975.

18. Haldar, A., and W.H. Tang, “Statistical Study of Uniform Cycles in Earthquake Motion”, Journal of the Geotechnical Engineering Division, ASCE, Vol. 107, No. GT5, pp. 577-589, 1981.
19. Pyke, R., H.B. Seed and C.K. Chan, “Settlement of Sands under Multidirectional Shaking”, Journal of the Geotechnical Engineering Division, Vol. 101, No. GT4, pp. 379-398, 1975.
20. Seed, H.B., K.L. Lee, I.M. Idriss and F.I. Makdisi, “The Slides in the San Fernando Dams During the Earthquake of February 9, 1971 ”, Journal of Geotechnical Engineering Division, ASCE, Vol. 101, No. GT7, pp. 651-688, 1975.
21. Sun, J. I., Golesorkhi, R., and Seed, H. B., “Dynamic moduli and damping ratios for cohesive soils,” Report No. EERC-88/15, Earthquake Engineering Research Center, University of California, Berkeley.
22. Seed, H. B., and Idriss, I. M., “Soil moduli and damping factors for dynamic response analyses,” Report No. EERC 70-10, Earthquake Engineering Research Center, University if California, Berkeley.